Research Article | Vol. 30, No. 16 / 1 Aug 2022 / Optics Express 28268

Optics EXPRESS

Ultra-lightweight mirrors with high solar reflectivity and high infrared emissivity for sun-facing radiative thermal management in space

SAMUEL LOKE, ALI NAQAVI, EMILY WARMANN, PILAR ESPINET-GONZALEZ, NINA VAIDYA, MICHAEL KELZENBERG, AND HARRY A. ATWATER*

Department of Applied Physics and Materials Science, California Institute of Technology, 1200 E California Blvd, Pasadena, CA 91125, USA

haa@caltech.edu

Abstract: We report the design, fabrication, and characterization of ultralight coatings that employ Salisbury screen principles and the unique nature of ITO to achieve frequency selective broadband emissivity. Our coating comprises 60 nm SiO_2, 10 nm ITO, 2.3 μm NeXolv LaRC CP1 polyimide and 300 nm Ag, and achieves an aerial mass of 4.07 gm^{-2}. It has a calculated and measured visible spectrum reflectivity of R = 0.893 and R = 0.896 respectively when weighted against AM0 from 300 nm to 1800nm; and a calculated and measured IR spectrum emissivity of e = 0.574 and e = 0.554 weighted against a 300 K blackbody respectively. This simple coating design, fabricated on the centimeter scale, achieves broadband frequency selectivity, with the highest reported thermal performance for an ultralight sun-facing radiative energy management structure.

1. Introduction

The design of surfaces to efficiently emit thermal radiation is an expanding area of research that has received considerable attention over the past decade [1,2,3], and has been accelerated by the ability to realize wavelength and subwavelength scale structures. The ability to tailor selective spectral emissivity profiles has enabled new solutions to challenges in thermal management [4,5,6]; an important technology with applications across a broad spectrum of industrial sectors. Thermal management is critical to durability and longevity of mechanical and electrical components and systems. Thermally emissive surfaces present an opportunity for components to passively cool themselves. This is especially important in space-based applications, where conduction and convection are unavailable as heat loss mechanisms.

Spacecraft and other deployable structures in space reach temperatures determined by the radiative flux balance between absorption and emission. In particular those positioned near the Earth have a side facing the Sun and a side that faces either the earth or cold space background. The side facing away from the Sun or the Earth loses heat easily via radiative means, as it is exchanging heat with the universe, which behaves as a blackbody at 3 K. This face will always be radiating heat and therefore cooling. The side that faces the Sun however, is exchanging heat radiatively with the 5778 K solar blackbody. If the mirror surface has nonzero absorptivity, it will gain heat. If cooling is desired, this surface is often a mirror surface that reflects most of the radiated power from 300 nm to 1800nm, where solar radiation is strongest, to avoid solar energy gain. This design criterion limits the solar heat gain but does not specify how to harness the Sun-facing side as a thermally emitting surface. Ideally, we also want both surfaces to be highly emissive over a wavelength range of 2 μm to 35 μm where a 300 K blackbody is most emissive.

#454212 https://doi.org/10.1364/OE.454212
Journal © 2022 Received 22 Feb 2022; revised 29 Apr 2022; accepted 3 May 2022; published 18 Jul 2022

Optics EXPRESS

Emissive surfaces in space thus can be designed to operate at temperatures near 300 K even under conditions of continuous solar irradiation. In other words, we seek to design structures whose Sun facing side is a frequency-selective surface that is both highly reflective in the visible spectrum of 300 nm to 1800nm and highly emissive in the infrared (IR) spectrum of 2 μm to 35 μm. For application to large-scale deployable space structures, such as those for space based solar power [6], we also require structures whose mass/area is extremely low, ideally < 10 g/m^2.

$$\varepsilon(\lambda) = \alpha(\lambda) = 1 - r(\lambda) - t(\lambda) \tag{1}$$

In Eq. (1), λ is wavelength, and ε, α, r and t are spectral emissivity, spectral absorptivity, spectral reflectivity and spectral transmission at wavelength λ. With this equation in mind, we consider the complexities of achieving a surface that is emissive in one wavelength regime, yet reflective in another. Previous designs have identified nanophotonic designs that have achieved such frequency selectivity but which either demand lengthy fabrication processes [7] or exhibit high aerial mass densities of ∼100 gm^{-}2 via use of 100 μm polymer structures [8] which have mass/area values that exceed the mass budget for deployable space structures. Other reports for highly emissive structures either involve considerable fabrication complexity, such as carbon nanotube fabric synthesis [9] or comprise thick applied coatings that also have excessive mass/area for space structure applications [1,3]. By contrast, simple planar metallodielectric have successfully demonstrated high emissivity structures and are both easy to fabricate over large areas, conceivably in a roll-to-roll process, and with subwavelength thicknesses and hence have potential for ultralightweight form factors [10]. These structures employ a metal-insulator-metal structure (MIM) known as a Salisbury screen [11], where the top metal layer is extremely thin, allowing partial reflection as well as partial transmission of light to the insulator region, which is of a thickness equal to a quarter of the peak wavelength of the desired absorption spectrum within the dielectric medium. This is so that the transmitted wavelength travels a half wavelength within the dielectric medium by the time it is reflected from the metallic back reflector and exits the insulator layer; so that the reflected wave is out of phase with the zeroth order reflected light causing destructive interference, effectively canceling reflection, increasing absorptivity and by reciprocity arguments also increasing the emissivity. While many previous reports of the Salisbury screen principle have validated the concept that careful selection of material for the top metal layer can yield a structure index matched to its free space surroundings, there are no reports to date indicating how to achieve these designs for thermal infrared energy management in ultralight structures, which has motivated the present design, fabrication, and characterization approach for ultralight and frequency-selective coatings that employ the Salisbury screen architecture for space-based thermal management.

2. Design and simulation

We begin with materials selection for our MIM Salisbury screen architecture. Previous work [12] has shown that the space-compatible polymer NeXolve LaRC-CP1 polyimide [13] has favorable near-to-mid IR emissivity properties that benefit our structure in this regime, where we desire broadband and high emissivity. As such we select this polymer for our quarter wave insulator region. For our desired visible response, the topmost thin metal layer and back reflector metal require some careful consideration. The topmost thin metal layer must be transparent in the visible regime yet reflective in the IR regime. As most metals experience a plasmonic resonance in the visible regime, this can be difficult to achieve. However, indium tin oxide (ITO) is one such material, as can be seen from its refractive index data plotted in Fig. 1. Comparing this to the refractive index of Cr plotted in Fig. 1, used in previous work [12], we see in ITO a material that is able to achieve the frequency selectivity we desire. Selecting the back reflector is a slightly easier task, both Ag and Al are suited for highly reflective mirror to increase visible spectrum reflectivity. However, Ag is more reflective than Al over a larger portion of the visible spectrum,

Optics EXPRESS

and as such we select Ag as our back reflector. Finally, we cap and encapsulate our coatings with a protective layer of SiO_2 to achieve the metasurface schematic shown in Fig. 2.

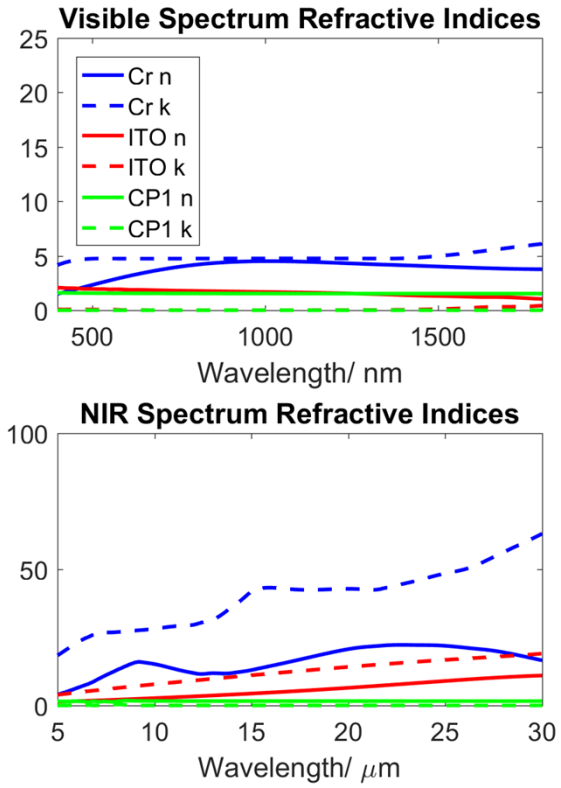

Fig. 1. Comparative plots of refractive index data for chromium, ITO and space-compatible polyimide CP1.

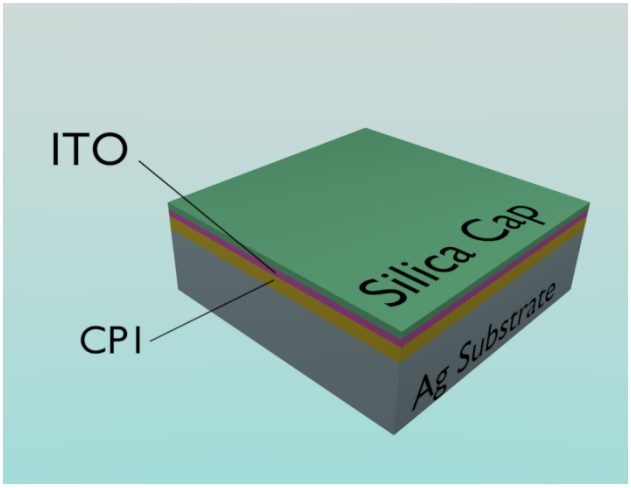

Fig. 2. Schematics of the Salisbury screen.

Optics EXPRESS

Before we begin discussing designing and fabricating our emissive coating, let us take some time to consider the implications the space environment has on our material selection. The first consideration is the radiative background of space, comprising, amongst others, energetic protons and electrons. The materials, ITO and CP1 [14][15], have both demonstrated to exhibit optical radiation hardness while Ag, being a metal, isn't damaged by space radiation as it can conduct the electrostatic influx away quickly. Second consideration is the temperature cycling of a body in space, especially one such as ours that will have a thin films of metal, polymer, and ceramics deposited on each other. It is here that we must remind ourselves of our coating's intended applications: that is, to say, our coating exists to maintain an operating temperature of around 300-350 K in sun-facing bodies expected to orbit the Earth constantly facing the Sun, such as geostationary orbits. Such application examples include space-based solar power (SBSP) as detailed in [6,16,17]. According to our past work on SBSP, our sun facing carbon-fiber-reinforced polymer (CFRP) space mirror design is able to maintain cell temperatures below 100 °C with low CFRP thicknesses (minimum of 37 μm) as long as a mirror emissivity of 0.3 - 0.6 can be achieved. In practice our prototype maintained an operating temperature of ~ 70 °C, i.e. ~ 343 K, under simulated AM0 solar illumination in ambient lab conditions. Drastic temperature cycles are not expected in the operation of our coatings and hence considerations of inter-film stress due to temperature cycling are outside the scope of this study.

Having established our materials, we begin our simulations to optimize and predict the behavior of our coating. Simulations were conducted via the RETICOLO code which uses the rigorous couple wave analysis (RCWA) technique [18]. First, the thicknesses of ITO and CP1 polyimide were varied to obtain the spectral visible regime reflectivity and IR regime emissivity. These were then weighted against air mass 0 (AM0) solar spectrum and a black body at 300 K respectively to give a measure of visible reflectivity and IR emissivity, using the formulae present in Eqs. (2) and (3).

$$R = \frac{\int I_{AM0}(\lambda) r(\lambda) d\lambda}{\int I_{AM0}(\lambda) d\lambda} \tag{2}$$

$$\varepsilon(300K) = \frac{\int I_{BB}(\lambda, 300K) \varepsilon(\lambda) d\lambda}{\int I_{BB}(\lambda, 300K) d\lambda} \tag{3}$$

where R is reflectivity, $r(\lambda)$ is spectral reflectivity, $I_{\mathrm{AM0}}(\lambda)$ is the AM0 intensity spectrum from 300 nm to 1800nm, ε is emissivity,$\varepsilon(\lambda)$ is spectral emissivity and $I_{\mathrm{BB}}(\lambda,300\ K)$ is the intensity spectrum of a 300 K blackbody from 2 μm to 35 μm.

The color plots in Fig. 3 give us a map that allows us to select our desired thicknesses. We wish to maximize IR emissivity without compromising visible reflectivity. This we find to be achievable at 10 nm of ITO and 2.3 μm of CP1, which results in a visible reflectivity of 0.893 and an IR emissivity of 0.574.

In order to develop a greater appreciation for our chosen parameters, consider Fig. 3 in greater detail. We notice that increasing ITO thickness reduces visible reflectivity while increasing IR emissivity. This we account easily via the Beer-Lambert Law [19] to state that more light is scattered through a thicker layer, resulting in higher absorptivity and hence lower reflectivity and higher emissivity. However, also to note is that IR emissivity falls above a certain thickness. This occurs because transmitted light intensity is not high enough to interfere with the zeroth order reflected light from the ITO coating.

This condition defines a maximum emissivity and in turn the optimal ITO thickness. However, as mentioned earlier, we also desire a high visible spectrum reflectivity, thus while the optimal ITO thickness is 20 nm from Fig. 3(b), we must aim for a thickness that can still achieve an IR emissivity of 0.5-0.6 without sacrificing the desired reflectivity. It is for this reason we have selected 10 nm of ITO for our structure, with the caveat that one can then tailor the ITO thickness to suit their optical needs better based on Fig. 3.

Optics EXPRESS

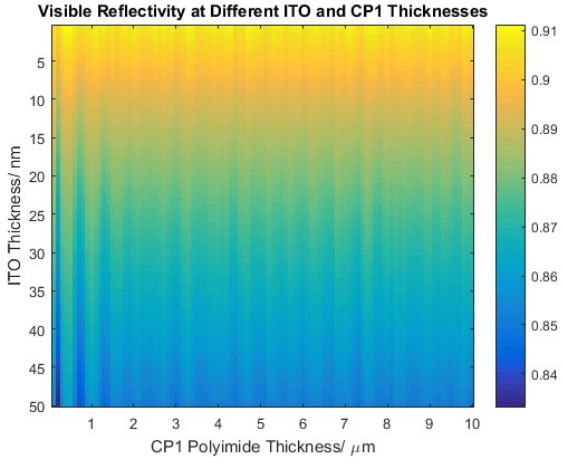

(a)

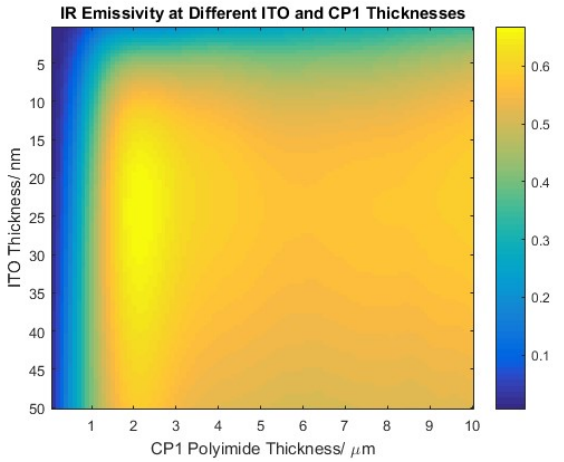

(b)

Fig. 3. Varying thicknesses of CP1 and ITO to optimize (a) visible spectrum reflectivity and (b) IR spectrum emissivity.

Optics EXPRESS

Varying CP1 thickness, we note fluctuating trends in both visible reflectivity and IR emissivity as interference occurs in the dielectric layer. As such, increasing CP1 thickness causes an alternation between a resonance mode due to constructive interference and an anti-resonance mode due to destructive interference at every wavelength. When weighted against AM0 and 300 K blackbody spectra, this results in the observed fluctuating reflectivity. However, there is an overall maximum in the IR emissivity at the chosen 2.3 μm CP1 thickness. The maximum in the 300 K blackbody emissivity occurs at around 10 μm, which corresponds to around 4 times the thickness of the layer, allowing for maximum absorptivity at the most intense region of a 300 K blackbody due to destructive interference arising from a subwavelength thickness structure. In the process of designing this emissive mirror coating, we selected the dielectric thickness to maximize IR emissivity over the desired spectrum.

To gain a more comprehensive understanding of the interactions between the layers in our coating, we conducted two sets of calculations summarized in Fig. 4. The first considers the contribution of each layer to spectral reflectivity and emissivity by looking at the absorption in each layer at every wavelength. Figure 4(a) plots the visible response while Fig. 4(b) plots the IR response. In Fig. 4(a) we see minimal losses, as we would hope for in the case of a visible spectrum mirror, and most losses occur due to the plasmonic resonance from Ag at the UV-Vis area of 300 nm to 400 nm. For the IR spectrum, in Fig. 4(b), we notice two types of absorptive effects: narrowband resonances from 2 μm to 10 μm, and a broadband absorption from 10 μm onwards. The narrowband resonances have been previously accounted for as an effect due to CP1 molecular vibrational bond resonances [6], however, we also notice some additional narrowband resonances arising from the ITO in this wavelength regime. The broadband effect is largely seen in the ITO layer, which would lead one to assume this occurs because of the lossy nature of ITO in the IR as most studies have also assumed [4]. However, one must turn to our next set of calculations to fully realize the broadband phenomena which is occurring.

Consider now the $|E|^2$ electric field profile in each layer. Figure 4(c) displays the normalized $|E|^2$ profiles across the depth of the coatings, at various important wavelengths. In order to have meaningful comparison, the depth profiles are not to scale. We see two distinct types of profiles here: highly reflective, resonant modes at wavelengths of 1400 nm and 1800nm where the $|E|^2$ profile in the CP1 layer expresses $n * \lambda / 2$ oscillations; and highly absorptive, anti-resonant modes at 1600 nm and well into the IR wavelengths where $|E|^2$ appears to have $(n + 1/2) * \lambda / 2$ oscillations, where the CP1-ITO boundary sees a maxima as opposed to a minima in the resonant case. We define these modes as resonant and anti-resonant by considering their relation and interference with the zeroth order reflection at the ITO-vacuum interface. Resonant modes yield a constructive interference of the first order and zeroth order reflection, while anti-resonant modes yield destructive interference as the first order reflection emerges out of phase with the zeroth order reflection [4]. Particularly, we notice how the profile observed at 15 μm is also observed at other, higher wavelengths, suggesting that the quarter wavelength cancellation effect, while at first glance a narrowband, anti-resonant effect, is actually a broadband effect at IR wavelengths as radiation with longer wavelengths still experience some degree of the destructive interference. One may think of it as though the reflected, interfering radiation exits with a phase difference just off of $\lambda/2$ which still reduces the strength of the zeroth order reflected light.

We also conducted angle-dependent analysis in both visible and IR spectra with two studies in mind. In studying the visible spectrum angle sensitivity, we evaluate the effectiveness of our mirror at all angles. In studying the IR spectrum angle sensitivity, we endeavor to find the angle-averaged emissivity of our coating by integrating over all angles under the Lambert cosine law that is given by Eq. (4).

$$\overline{\varepsilon} = \frac{\int \cos\theta \int I_{BB}(\lambda, 300K)\varepsilon(\lambda, \Omega) d\lambda d\Omega}{\int \cos\theta \int I_{BB}(\lambda, 300K) d\lambda d\Omega} \tag{4}$$

Optics EXPRESS

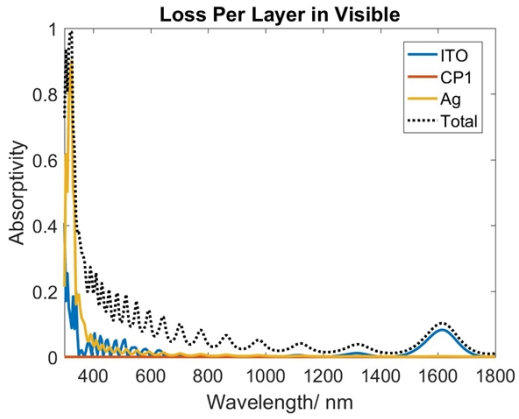

(a)

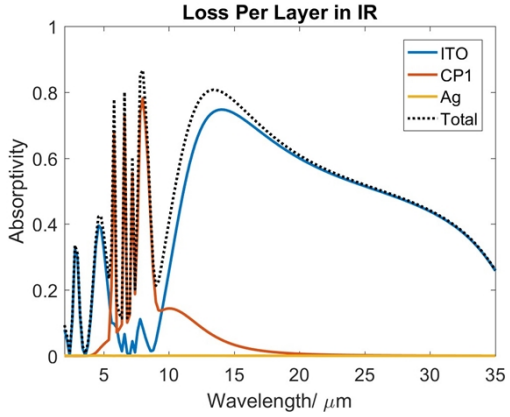

(b)

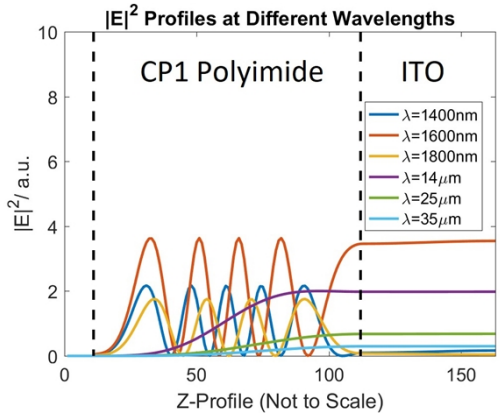

(c)

Fig. 4. Layer-by-layer calculation of (a) visible spectrum reflectivity and (b) IR spectrum emissivity. and as such the amount of shorter wavelength that gets cancelled is less.

Optics EXPRESS

In order to do this, assuming in-plane isotropy of our coating, we calculate the visible reflectivity and IR reflectivity at incident angles going from 0° to 90°. We plot TM and TE polarizations, as well as the average of the two, in Fig. 5. We note across the visible spectrum that the reflectivity actually increases at higher angles, with observable absorptivity oscillations at angles greater than 60°. At higher angles, the quarter wavelength condition is met for longer wavelength radiation as the path travelled by the beam is longer.

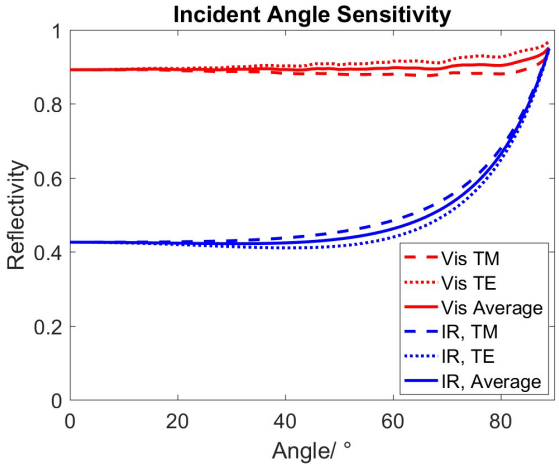

Fig. 5. Plot of reflectivity against angle.

We thus conclude that our surface acts as a good visible spectrum mirror at all angles. TM-polarized light is generally absorbed more than TE-polarized light, in agreement with the Fresnel equations. We see a similar trend in the IR, and report angle insensitivity up to around 60°. We note also the Brewster's angle resulting in maximum absorption of TM-polarized light at around 60°. Using Eq. (4), we find the angle-averaged emissivity to be $e = 0.544$. As a final measure, we also calculate that such a structure will have an areal density of 4.073 gm^{-2}, which is comparable to our previous work where we presented a Salisbury screen with angle-averaged emissivity of 0.6 and an areal density of 3.3 gm^{-2} [12].

3. Experimental

Samples were fabricated on a Si wafer. 200 nm of Ag was deposited on the Si wafer via electron beam evaporation. 1.3 ml of CP1 resin was mixed with 2.7 ml of diglyme (1-methoxy-2-(2-

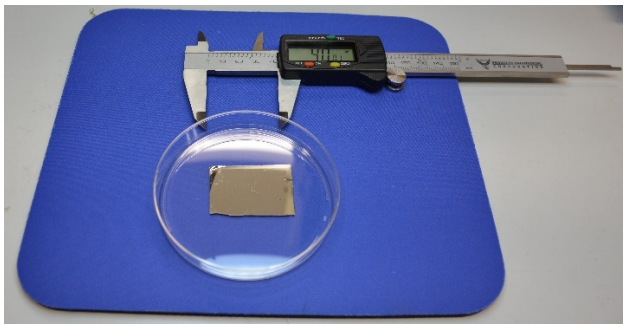

Fig. 6. Image of the fabricated Salisbury screen.

Optics EXPRESS

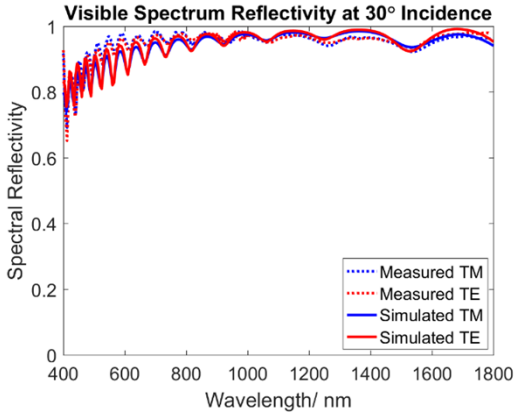

(a)

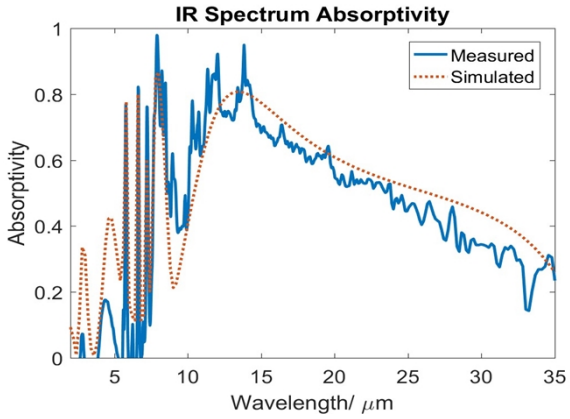

(b)

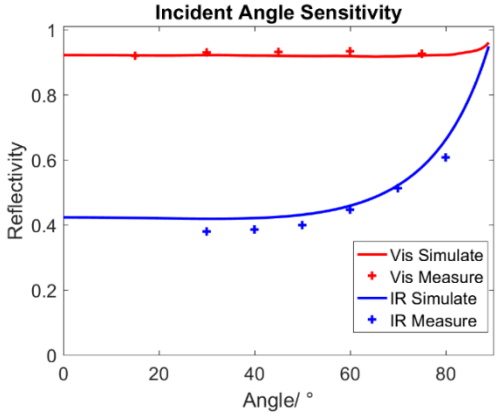

(c)

Fig. 7. Comparing measurements against calculations. a) visible spectrum at 30 incident angle; b) IR spectrum at 30 incident angle; c) incident angle sweep.

Optics EXPRESS

methoxyethoxy)ethane) solvent and spin-coated on Ag at 1000 rpm. 10 nm of ITO was then deposited via sputtering, and finally a 60 nm SiO_2 capping layer was deposited via electron beam deposition. The final surface is presented in Fig. 6.

Reflectivity measurements were then conducted via UV-Vis and IR ellipsometry. Reflectivity was measured at the lowest possible angle of incidence achievable with our experimental setup, 30°. The reflectivity of the sample was measured in the wavelength range of 300 nm to 1800nm in the UV-Vis ellipsometer and 2 μm to 35 μm in the IR ellipsometer. The visible spectrum reflectivity and mid-IR emissivities are then plotted in Fig. 7(a) and Fig. 7(b) respectively, alongside the simulations. We report a measured visible reflectivity of 0.896 and measured IR emissivity of 0.554. We then conduct an angle sweep from 40 to 80 using both the UV-Vis and IR ellipsometers, and plot our measured reflectivities against the calculated ones in Fig. 7(c). We find our experimental results to be in agreement with our simulations, with key resonant and interference features being observed at the appropriate wavelengths.

4. Conclusion

In conclusion, we present the design, fabrication and characterization of ultralight and frequency-selective metasurfaces that both high solar reflectivity and infrared emissivity. Our design is based on the MIM Salisbury screen architecture. These surfaces are easy to fabricate over centimeter scales, requiring few deposition steps and no lithography. These surfaces are highly reflective in the visible, possessing calculated and measured reflectivities of $R = 0.893$, and $R = 0.896$ respectively when weighted against AM0 from 300 nm to 1800nm; and are also highly emissive in the IR, possessing calculated and measured emissivities of $e = 0.574$, and $e = 0.554$ when weighted against a 300 K blackbody from 2 μm to 35 μm. We account this unique set of radiative characteristics to the combination of an effective lightweight broadband absorber structure in the Salisbury screen, ITO's unique refractive index, and CP1's near-IR set of resonances. In addition, our structure is fairly angle-insensitive and is lightweight, having an areal density of 4.07 gm^{-2} thanks to its subwavelength thickness. This combination of characteristics makes our surface an excellent candidate for several ultralight space-based applications, most notably we highlight, as a Sun-facing cooling surfaces for space-based thermal management.

Funding. Space Solar Power Project.

Acknowledgements. The authors wish to acknowledge Tom Tiwald for characterizing the optical properties of polymer CP1 in our previous work.

Disclosures. The authors declare that there are no conflicts of interest related to this article.

Data availability. The data is not publicly available at this time but may be obtained from authors upon request

References

1. Y. Zhai, Y. Ma, S.N. David, D. Zhao, R. Lou, G. Tan, R. Yang, and X. Yin, "Scalable-manufactured randomized glass-polymer hybrid metamaterial for daytime radiative cooling," Science **355**(6329), 1062–1066 (2017).
2. S.Y. Jeong, C.Y. Tso, Y.M. Wong, C.Y. Chao, and B. Huang, "Daytime passive radiative cooling by ultra emissive bio-inspired polymeric surface," Sol. Energy Mater. Sol. Cells **206**, 110296 (2020).
3. J. Mandal, Y. Fu, A.C. Overvig, M. Jia, K. Sun, N.N. Shi, H. Zhou, X. Xiao, N. Yu, and Y. Yang, "Hierarchically porous polymer coatings for highly efficient passive daytime radiative cooling," Science **362**(6412), 315–319 (2018).
4. T. Li, Y. Zhai, S. He, W. Gan, Z. Wei, M. Heidarinejad, D. Dalgo, R. Mi, X. Zhao, J. Song, and J. Dai, "A radiative cooling structural material," Science **364**(6442), 760–763 (2019).
5. L. Zhu, A. Raman, K.X. Wang, M.A. Anoma, and S. Fan, "Radiative cooling of solar cells," Optica **1**(1), 32–38 (2014).
6. E.C. Warmann, P. Espinet-Gonzalez, N. Vaidya, S. Loke, A. Naqavi, T. Vinogradova, M. Kelzenberg, C. Leclerc, E. Gdoutos, S. Pellegrino, and H.A. Atwater, "An ultralight concentrator photovoltaic system for space solar power harvesting," Acta Astronaut. **170**, 443–451 (2020).
7. E. Rephaeli, A. Raman, and S. Fan, "Ultrabroadband photonic structures to achieve high-performance daytime radiative cooling," Nano Lett. **13**(4), 1457–1461 (2013).
8. J.L. Kou, Z. Jurado, Z. Chen, S. Fan, and A.J. Minnich, "Daytime radiative cooling using near-black infrared emitters," ACS Photonics **4**(3), 626–630 (2017).

Optics EXPRESS

9. K. Mizuno, J. Ishii, H. Kishida, Y. Hayamizu, S. Yasuda, D.N. Futaba, M. Yumura, and K. Hata, "A black body absorber from vertically aligned single-walled carbon nanotubes," Proc. Natl. Acad. Sci. **106**(15), 6044–6047 (2009).
10. H. Kocer, S. Butun, Z. Li, and K. Aydin, "Reduced near-infrared absorption using ultra-thin lossy metals in Fabry-Perot cavities," Sci. Rep. **5**(1), 8157 (2015).
11. B. Chambers, "Optimum design of a Salisbury screen radar absorber," Electron. Lett. **30**(16), 1353–1354 (1994).
12. A. Naqavi, S.P. Loke, M.D. Kelzenberg, D.M. Callahan, T. Tiwald, E.C. Warmann, P. Espinet-González, N. Vaidya, T.A. Roy, J.S. Huang, and T.G. Vinogradova, "Extremely broadband ultralight thermally-emissive optical coatings," Opt. Express **26**(14), 18545–18562 (2018).
13. A.K.S. Clair and T.L.S. Clair, "Process for preparing essentially colorless polyimide film containing phenoxy-linked diamines," U.S. Patent 4,595,548. (1986).
14. D.V. Morgan, A. Salehi, Y.H. Aliyu, R.W. Bunce, and D. Diskett, "Radiation damage in indium tin oxide (ITO) layers," Thin Solid Films **258**(1-2), 283–285 (1995).
15. P.B. Willis, "Survey of radiation effects on materials," *Proc. Outer Planets Flagship Mission Instrum. Workshop*, pp. 5–8. 2008.
16. M.D. Kelzenberg, P. Espinet-Gonzalez, N. Vaidya, E.C. Warmann, A. Naqavi, S.P. Loke, P. Saive, T.A. Roy, T.G. Vinogradova, C. Leclerc, and E.E. Gdoutos, "Ultralight energy converter tile for the space solar power initiative," *2018 IEEE 7th World Conference on Photovoltaic Energy Conversion (WCPEC)(A Joint Conference of 45th IEEE PVSC, 28th PVSEC & 34th EU PVSEC)*, pp. 3357–3359. IEEE, 2018.
17. N. Vaidya, M.D. Kelzenberg, P. Espinet-Gonzalez, T.G. Vinogradova, J.S. Huang, C. Leclerc, A. Naqavi, E.C. Warmann, S. Pellegrino, and H.A. Atwater, "Lightweight carbon fiber mirrors for solar concentrator applications," *2017 IEEE 44th Photovoltaic Specialist Conference (PVSC)*. IEEE, 2017.
18. J.P. Hugonin and P. Lalanne, "Reticolo software for grating analysis," Institut d'Optique, Orsay France (2005).
19. J.D. Ingle Jr and S.R. Crouch, "Spectrochemical analysis," (1988).